Proceedings 10th NUMGE 2023
10th European Conference on Numerical Methods in Geotechnical Engineering
Zdravkovic L, Kontoe S, Taborda DMG, Tsiampousi A (eds)

https://doi.org/10.53243/NUMGE2023-178

A coupled-hyperelastic constitutive approach for modelling the mechanical behaviour of crushable granular soils

N. Irani[1], M. Tafili[1], L.F.Prada-Sarmiento[2], T. Wichtmann[1]

[1] *Chair of Soil Mechanics, Foundation Engineering and Environmental Geotechnics, Ruhr-University, Bochum, Germany*

[2] *Department of Civil and Architectural Engineering, Aarhus University, Denmark*

ABSTRACT: Particle breakage plays a fundamental role in the mechanical response of specific granular materials, and the corresponding effects could be incorporated into finite element simulations. Hence, accurate constitutive models are required for the mechanical description of soils with breakable grains. This study presents a hyperelastic constitutive model, which predicts the elastic response of crushable granular soils in a thermodynamically consistent frame. A revised free energy function is employed to derive the hyperelastic description of the material within the yield surface, incorporating an internal variable representing the particle size. In order to quantify the extent of particle breakage, a breakage index as a function of plastic shear strain and void ratio is used. The breakage index acts as a coupling variable by capturing the effect of plastic strain on the elastic properties of the soil in terms of an elastoplastic coupling mechanism. The performance of the new constitutive formulation in terms of response envelopes has been compared to experimental results on Karlsruhe Fine Sand (KFS).

Keywords: Hyperelasticity; Particle breakage; Breakage index; Hyperelastoplastic coupling.

1 INTRODUCTION

Particle breakage is considered a common process in some granular materials (Xiao et al., 2014a, Yu, 2017), particularly when subjected to relatively high-stress levels or high loading rates (Yamamuro & Lade, 1996; Mun & McCartney, 2017; Hyodo et al., 2017). Particle breakage alters the size (Cil & Alshibli, 2014; Karatza et al., 2019), shape (Zhang et al., 2021), and grain size distribution of soils (Xiao et al., 2016; Yu, 2019), which influences their mechanical behaviour under different loading paths. Ignoring particle breakage effects in the numerical simulations may result in inaccurate descriptions of the soil's response with possible consequences on the stability, strength (as particle breakage reduces the strength and mobilised friction angle (Hosseininia & Mirghasemi, 2007)) and deformation (as soil response changes from dilative to contractive one in the presence of breakage (Xiao et al., 2016)) of the soils. Thereby, the corresponding effects of the breakage process have to be incorporated into finite element simulations. In consequence, the mechanical behaviour of soils with breakable grains must be accurately described by new or modified constitutive equations.

In conventional continuum modeling of granular materials, both elastic and plastic parts of behaviour have been widely considered essential representing the deformation and stress transmission within a granular assembly. Elasticity theories in continuum mechanics are categorized into two branches including hyperelasticity and hypoelasticity. The mentioned classification of the elastic stiffness tensor of materials is normally based on the accumulation of stress and energy after a closed strain path loop. Although the mathematical simplicity of a hypoelastic framework is appealing, it contravenes the second law of thermodynamics and as a result, an effective closed stress path may not result in a closed elastic strain loop (Borja et al., 1997; Houlsby et al., 2005). Consequently, elastic strain accumulation may occur with hypoelastic constitutive equations under cyclic loading even of a small amplitude, whereas in a hyperelastic approach, it is possible to predict a closed loop cycle of effective stress within a framework that conserves energy (Irani et al., 2022). This leads to a substantial improvement in predicting the soil behaviour under cyclic loading. To the best knowledge of the authors, only a few soil constitutive models have been developed for the simulation of crushable soil response in an energy-conservative frame, which highlights the requirement of the hyperelastic frames for soils with breakable grains.

The main objective of this study is to simulate the elastic response of crushable soils in a thermodynamically consistent frame. To achieve this, hyperelastic constitutive equations are derived based on a revised free energy function. A breakage index postulated as a function of plastic shear strain and void ratio is employed to quantify the breakage extent of specimens under shear-loading. The plastic shear strain is calculated using a bounding surface plasticity model. In order to evaluate the proposed formulation, a series of response envelopes of sand are simulated.

2 FUNDAMENTALS OF HYPERELASTIC CONSTITUTIVE EQUATIONS

When a load is applied to a crushable soil assembly, the smaller particles are placed around larger particles and do not contribute to the load-transfer mechanism (Einav, 2007a; Tafili et al., 2022); consequently, they do not store energy (Einav, 2007a). The energy potentials are in this case expected to include an internal variable related to particle size, in addition to the conventional variables (say the invariants of stress or strain tensor). This internal variable can represent the changes in the microstructure and particle arrangement that occur due to variations in particle size. To achieve this, Einav (2007a,b) introduced a general formulation of the Helmholtz potential that considers the influence of particle size. Assuming the gradation curve as a weighted average function over microscopic variables, the Helmholtz potential was expressed in terms of the elastic strain invariants and a breakage index. Geotechnical engineers commonly prefer to initialize the stiffness tensor in terms of stress, because it is easier to infer the natural in-situ stress state than knowing the corresponding initial strain state. As a result, a Gibb's potential function based on isomorphic stress invariants (P and Q, where the true magnitude and direction of vectors are preserved) and breakage index (B) is here expressed as follows:

$$\psi = \psi_r(P,Q)\cdot(1-\upsilon B) \tag{1}$$

where $\psi_r(P,Q)$ is the energy function for zero particle breakage and υ is a model parameter. Considering $\boldsymbol{T}$ and $\boldsymbol{T}^* = \boldsymbol{T} - \frac{-\mathrm{tr}\boldsymbol{T}}{3}\mathbf{1}$ as the Cauchy stress tensor and its deviatoric part, respectively, the isomorphic invariants $Q = \|\boldsymbol{T}^*\| = \sqrt{\boldsymbol{T}^*:\boldsymbol{T}^*}$ and $P = \frac{-tr\boldsymbol{T}}{3}$ are defined. $\mathrm{tr}\boldsymbol{T}$ denotes the trace of the stress and $\mathbf{1}$ is the second-order identity tensor. The elastic strain ($\boldsymbol{\varepsilon}^e$) can be calculated using the first derivative of the energy potential with respect to the stress tensor as:

$$\varepsilon^e_{ij} = \frac{\partial\psi}{\partial\boldsymbol{T}} = \frac{\partial\psi_r}{\partial\boldsymbol{T}}(1-\upsilon B) + \frac{\partial(1-\upsilon B)}{\partial\boldsymbol{T}}\psi_r \tag{2}^{a}$$

The rate of elastic strain tensor can be calculated using differentiation of Eq. (2)[a] as:

$$\dot{\varepsilon}^e_{ij} = \underbrace{\frac{\partial^2\psi}{\partial T_{ij}\partial T_{kl}}\dot{T}_{kl}}_{\text{(I)}} + \underbrace{\frac{\partial^2\psi}{\partial T_{ij}\partial B}\dot{B}}_{\text{(II)}} \tag{2}^{b}$$

According to Eq. (2)[b], the total elastic strain rate is a function of stress and breakage index. Breakage is an irreversible process (Guo & Zhu, 2017); the incorporation of $\dot{B}$ in Eq. (2)[b] now influences the elastic response of crushable soils. In this sense, the total elastic strain rates in Eq. (2)[b] are decomposed into two terms: (I) the reversible term upon effective stress reversal, and (II) the irreversible term depending on breakage rates. Relating the breakage index to a proper hardening variable, B increases gradually with plastic strain in the elastoplastic domain of the behavior and remains unchanged ($\dot{B}=0$) as long as the soil behaves purely elastic. Thereby, the elastic strain rates in Eq. (2) are decomposed as follows:

$$\dot{\varepsilon}^e_{ij} = \dot{\varepsilon}^{er}_{ij} + \dot{\varepsilon}^{ei}_{ij} \tag{2}^{c}$$

wherein superscripts "*er*" and "*ei*" denote, respectively, the reversible and irreversible parts of the strain rates. The total strain rate for materials with possible coupling between the elastic and plastic strain rates is illustrated in Table 1. The coupling between elasticity and plasticity in the mechanical response of soils has been addressed in previous studies (Gajo et al., 2001; Golchin & Lashkari, 2014) demonstrating that plastic strain history of soils affects their elastic properties.

The compliance tensor ($\mathbf{C}$) can be calculated through the second derivative of Eq. (2)[a] as:

$$\begin{aligned}\mathrm{C}_{ijkl} &= \frac{\partial^2\psi}{\partial\boldsymbol{T}\partial\boldsymbol{T}} \\ &= \frac{\partial^2\psi_r}{\partial\boldsymbol{T}\partial\boldsymbol{T}}(1-\upsilon B) + 2\cdot\frac{\partial(1-\upsilon B)}{\partial\boldsymbol{T}}\frac{\partial\psi_r}{\partial\boldsymbol{T}} \\ &\quad + \frac{\partial^2(1-\upsilon B)}{\partial\boldsymbol{T}\partial\boldsymbol{T}}\psi_r\end{aligned} \tag{3}$$

The inverse of the compliance in Eq. (3) is the stiffness tensor (say $\mathrm{E}_{ijkl} = \mathrm{C}_{ijkl}{}^{-1}$). Thereby, a non-singular compliance matrix is desirable to calculate the stiffness matrix via numerical inversion. A stiffness matrix with a non-zero determinant (say det(E) > 0) or non-negative eigenvalues satisfies this condition (Prada, 2011; Irani et al., 2023a).

Table 1 Equivalent strain rates for elastoplastic coupled models (Collins and Houlsby, 1997)

Total strain rate	$\dot{\varepsilon}$		
[elastic+plastic] strain rate	$\dot{\varepsilon}^e$		$\dot{\varepsilon}^p$
[reversible elastic + irreversible elastic+ plastic] strain rate	$\dot{\varepsilon}^{er}$	$\dot{\varepsilon}^{ei}$	$\dot{\varepsilon}^p$
[reversible elastic+irreversible] strain rate	$\dot{\varepsilon}^{er}$	$\dot{\varepsilon}^i$	

The concept introduced here can be used as a foundation for the further development of more comprehensive granular models. For example, the elastic part of the bounding surface model (e.g., the SANISAND family of models) can be enriched by employing the hyperelastic formulation accounting for thermodynamic rules as well as a form of elastoplastic coupling; particularly

suited for granular soils with grains that are prone to break.

2.1 A hyper-elastic formulation accounting for particle breakage

A modified form of the potential proposed by Ashkar and Lashkari (2014) with the purpose of incorporating the particle breakage is adopted here:

$$\psi = \psi_r(P,Q)\cdot(1-\upsilon B) = \underbrace{\left[\frac{p_{\mathrm{ref}}}{(2-\chi)\bar{K}}V^{2-\chi}+\frac{Q^2}{4p_{\mathrm{ref}}\bar{G}}V^{-2\chi}\right]}_{\psi_r(P,Q)}(1-\upsilon B) \quad (4)^{a}$$

with

$$V=\frac{1}{2p_{\mathrm{ref}}}\left(\frac{3P}{\sqrt{3}}+\sqrt{\frac{P^2}{3}+\frac{\chi\bar{K}Q^2}{\bar{G}}}\right) \quad (4)^{b}$$

wherein p_{ref} and χ are constants. $\bar{G}=G_0F(e)$ and $\bar{K}=K_0F(e)$ are non-dimensional parameters dependent on the void ratio *e* with $F(e)=(2.97-e)^2/(1+e)$ proposed by Hardin and Richart (1963). G_0 and K_0 are material constants. This potential has been thoroughly evaluated by Irani et al. (2023a) in terms of the desired degree of homogeneity, as well as representing a positive and non-singular stiffness in the application range. It turned out, that the potential in Eq. 4 fulfils the primary restrictions.

Employing an appropriate breakage index for quantifying the amount of particle breakage during the loading process is required at this stage. According to Eq. (2) and Eq. (3), the extension of the breakage index is indispensable regarding the generalization of the constitutive equations into full tensorial domain. Adopting a breakage index independent of the stress invariants simplifies the formulation because in that form the index would not contribute to the first and second derivatives of the energy potential (i.e., the last two terms in Eq. (3) and the second term in Eq. (2) become zero). Thereby, the breakage index proposed by Irani et al. (2023b) is adopted here, expressed in terms of plastic shear strain (ε_q^p) and the void ratio (*e*) as follows:

$$B=1-\exp\left[-b\left(\frac{\varepsilon_q^p}{e}\right)^2\right] \quad (5)$$

where b is a material constant. Combination of Eq. (3) and Eq. (4), as well as substitution of the first and second derivatives of the stress invariants in Eq. (4) results in the following relation for the compliance tensor:

$$\mathrm{C}_{ijkl}=(1-\upsilon B)\left[\frac{\partial^2\psi_r}{\partial P\partial P}(-\vec{\mathbf{1}})(-\vec{\mathbf{1}})+ -\frac{\partial^2\psi_r}{\partial P\partial Q}\left[\vec{\mathbf{1}}\,\overrightarrow{\boldsymbol{T}^*}+\overrightarrow{\boldsymbol{T}^*}\,\vec{\mathbf{1}}\right]+\frac{\partial\psi_r}{\partial Q}\frac{1}{\|\boldsymbol{T}^*\|}\boldsymbol{D} +(\overrightarrow{\boldsymbol{T}^*})(\overrightarrow{\boldsymbol{T}^*})\left(\frac{\partial^2\psi_r}{\partial Q\partial Q}-\frac{1}{\|\boldsymbol{T}^*\|}\frac{\partial\psi_r}{\partial Q}\right)\right] \quad (6)$$

where $\boldsymbol{D}=\boldsymbol{J}-\vec{\mathbf{1}}\,\vec{\mathbf{1}}$ is a fourth-order deviatoric tensor; $J_{ijkl}=\delta_{ik}\,\delta_{jl}$ is the fourth-order identity tensor; $\vec{\mathbf{1}}$ is the normalised identity vector; δ is the Kronecker delta, and $\overrightarrow{\boldsymbol{T}^*}=\boldsymbol{T}^*/Q$ is the normalised deviatoric stress tensor. Table 2 summarizes the required first and second derivatives of stress tensor invariants. The calculation of the first and second derivatives could account for the dependency of energy potential on the void ratio, thus taking into account the relationship between *e* and stress invariants. For simplifying the constitutive equations, the terms pertaining to the first and second derivatives of the void ratio with respect to stress invariants are disregarded and left out for improvement in future works.

Table 2 Derivatives of stress invariants

Stress Invariant	First derivative	Second derivative
$\boldsymbol{P}=\frac{-\boldsymbol{trT}}{\mathbf{3}}$	$\frac{\partial P}{\partial \boldsymbol{T}}=-\vec{\mathbf{1}}$	$\frac{\partial^2 P}{\partial \boldsymbol{T}\partial \boldsymbol{T}}=0$
$\boldsymbol{Q}=\|\boldsymbol{T}^*\|$	$\frac{\partial Q}{\partial \boldsymbol{T}}=\overrightarrow{\boldsymbol{T}^*}$	$\frac{\partial^2 Q}{\partial \boldsymbol{T}\partial \boldsymbol{T}}=\frac{1}{\|\boldsymbol{T}^*\|}\left[\boldsymbol{D}-\overrightarrow{\boldsymbol{T}^*}\,\overrightarrow{\boldsymbol{T}^*}\right]$

3 EVALUATION OF THE PROPOSED MODEL

The performance of the proposed constitutive equations considering and ignoring the breakage process is evaluated in this section. For the first step, the constitutive equations are evaluated at zero breakage. The response envelopes determined from a series of triaxial tests on Karlsruhe Fine Sand (KFS) reported by Knittel et al. (2020) are employed to evaluate the performance of the potential in Eq. $(4)^{a}$ without considering the breakage effect (say considering which is the free energy function for B=0). The concept of response envelopes (Gudehus, 1979; Gudehus and Mašín, 2009) refers to a graphical representation of the soil stiffness under various loading directions. Knittel et al. (2020) performed a series of cyclic drained triaxial tests under relatively low strain increments (less than 2×10^{-4}) of the same length which were applied in different directions at various stress ratios and mean stresses. The resultant stress increments were plotted in the form of response envelopes. The motivation for simulating such tests is to evaluate the elastic stiffness of the soil under the different directions of strain increments based on the energy function proposed in Eq. (4). In addition, the potential with consideration

of the breakage variable was used for a series of qualitative simulations to assess the influence of the elastic stiffness response of the model under different loading directions. Due to the lack of experimental data on the response envelopes of crushable soils, this investigation is limited to a qualitative/theoretical analysis. Table 3 illustrates the set of constants used for the simulations.

Table 3. The model constants used for the simulations

Hyperelastic formulation (B=0)	Hyperelastic formulation ($B\neq0$)	Hypoelastic part of Dafalias and Manzari model (2004)
$G_0 = 150$	$G_0 = 150$	$G_0 = 150$
$K_0 = 90$	$K_0 = 90$	$\nu = 0.18$
$\chi = 0.5$	$\chi = 0.5$	
$\upsilon = 0$	$\upsilon = 0.5$	
	$b = 0.97$	

3.1 *Evaluation of the hyperelastic formulation neglecting the breakage process*

Figure 1 illustrates a comparison between simulations of response envelopes using the potential without breakage and experimental data performed by Knittel et al. (2020) on KFS. The response polars' shape and the rotation of major and minor axes agree well with experimental data, reflecting the ability of the hyperelastic potential to account for anisotropic stress states as well as for the influence of different mean effective stresses. The simulated response envelopes in triaxial compression and extension do not exhibit abrupt changes on their shape (convexity is preserved even for higher stress ratios) nor unacceptable discontinuities. Additionally, the inclination of the response ellipses increases as the stress ratio increases, which is well replicated by the constitutive equations.

3.2 *Evaluating the hyperelastic formulation considering breakage*

Figure 2 presents the calculated response envelopes activating the breakage term in the definition of the hyperelastic formulation, see Eq. (4)[b]. The results indicate that in principle the shape and the rotation of the major and minor axes of the calculated response envelopes are consistent with the experimental trends observed for KFS without particle breakage. Worth of note, is the squeezed shape of the response envelopes for anisotropic stress states approaching the critical state, while introducing breakage.

In hypoelastic approaches, the second law of thermodynamics is not upheld, as a result, a closed strain loop does not result in a closed effective stress path and vice versa. To investigate this analytically, the proposed hyperelastic constitutive equations have been coupled with the bounding surface plasticity model presented in Dafalias and Manzari (2004). The new model was implemented in full tensorial version in umat subroutine, and the following simulations are conducted using the Incremental Driver software (Niemunis, 2008). Thereby, as an element-type simulation a single Gauss point finite element is considered.

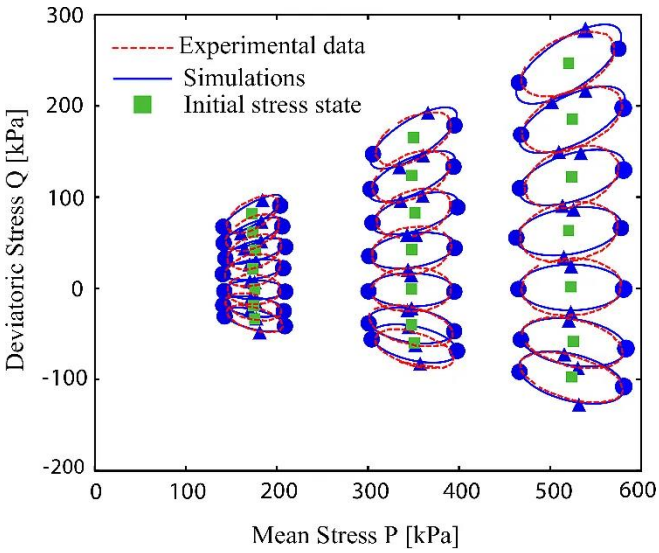

Figure 1Comparison between response envelopes of KFS simulated using the potential in Eq. 2 and experimental data performed by Knittel et al. (2020), blue dots denote isotropic compression and extension, while the triangles denote deviatoric compression and extension.

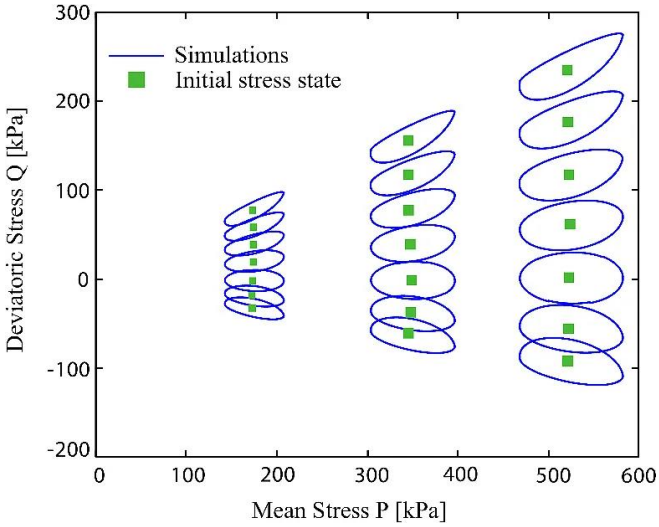

Figure 2 Response envelopes simulated using the hyperelastic model considering the breakage-induced process.

100 closed strain cycles with small amplitude were prescribed. The vertical and horizontal strain components, ε_{11} and ε_{22}, respectively, were defined as harmonic functions of time (t), with a time increment Δt = 1 s:

$$\varepsilon_{11}(t) = 2\,\pi\varepsilon_{\text{amp}}\cos\left(\frac{2\pi}{\Delta t}\right)$$
$$\varepsilon_{22}(t) = 2\,\pi\varepsilon_{\text{amp}}\cos\left(\frac{2\pi}{\Delta t} + \omega\right) \quad (7)$$

where ω and ε_{amp} are the initial phase and strain amplitude, respectively. $\varepsilon_{amp} = 10^{-5}$ and $\omega = \frac{\pi}{3}$ were assumed. The results of the element test simulations using the hypoelastic-plastic model (say the bounding surface plasticity model of Dafalias & Manzari, 2004) and the hyperelastic-plastic model (say the proposed hyperelastic approach coupled with the bounding surface plasticity model of Dafalias & Manzari, 2004) are presented in the isomorphic P-Q plane in Fig. 3. When coupling the hyperelastic formulation with bounding surface plasticity, the soil response can be captured in an energy-conserving frame within the yield surface. Once the yield surface is reached, plasticity is generated, and the soil response is simulated in a hyperelastic-plastic framework. Two constants are required for the description of hypoelasticity, namely the Poisson Ratio (ν) and G_0 with the corresponding values presented in Table 4. The remaining parameters in Table 4 represent bounding surface plasticity constants which have been employed from the constants determined for KFS by Wichtmann et al. (2019). The direction of the plastic strain increment tensor is defined by the flow rule.

Figure 3b shows that a hypoelastic stiffness may lead to a numerical accumulation of stress, whereas the hyperelastic-plastic approach predicts a fully reversible response (i.e., a closed stress loop after 100 cycles as seen in Figure 3c). However, when the number of cycles is high (N>100), small computational inaccuracies can add up and diminish the benefits of the hyperelastic approach.

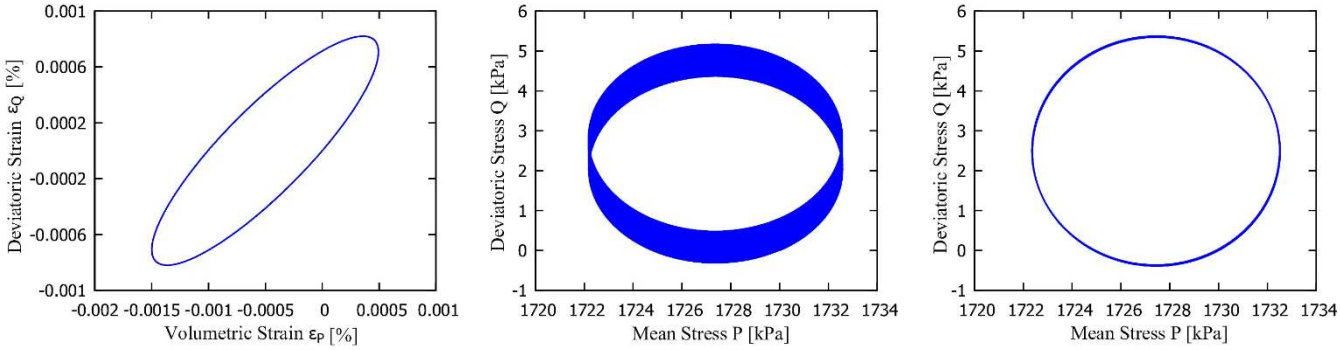

(a) (b) (c)

Figure 3 Model response under the application of package of (a):100 closed strain cycles using (b): The bounding surface plasticity model proposed by Dafalias and Manzari (2004) (c): The proposed hyperelasic formulation coupled with the bounding surface plasticity model of Dafalias and Manzari (2004)

Table 4 The material constants of bounding surface plasticity model of Dafalias & Manzari (2004) used for the simulations

e_0 [-]	λ [-]	ξ [-]	M_c [-]	M_e [-]	m [-]	h_0 [-]	c_h [-]	n_b [-]	A_0 [-]	n_d [-]	z_{max} [-]	c_z [-]
1.103	0.122	0.205	1.34	0.94	0.05	10.5	0.75	1.2	0.9	2.0	20.0	10^4

4 CONCLUSIONS

This study presented a hyperelastic constitutive model for granular soils, which considers the effects of particle breakage on the elastic response of soils. The proposed model includes a breakage index acting as a coupling variable to capture the influence of plastic strain on the elastic properties of the soil. The results showed that the new model can quantitatively well predict the response envelopes of sand compared to experimental data without breakage. Unfortunately, there is a lack in the literature with comparable data on granular materials with grains susceptible to crushing. Nevertheless, the quantitative simulations show that the modelled response envelopes become squeezed in shape for stress states approaching the critical state.

To illustrate the advantage of the hyperelastic stiffness tensor, 100 closed elastic strain cycles have been simulated with the bounding surface plasticity model of Dafalias and Manzari (2004) considering the original hypoelastic stiffness and the proposed model coupled with this bounding surface model. As expected, the involvement of a hypoelastic frame in the numerical simulation of element tests resulted in a numerical accumulation of stress, whereas closed stress cycles (i.e., fully reversible response) were obtained using the proposed hyperelastic formulation. Nonetheless, it remains unverified whether computational errors will affect these results for a greater number of cycles.

5 REFERENCES

Ashkar Z, Lashkari A (2014). A hyperelastic theory for granular soils and its application. In: 2nd Iranian Conference on Geotechnical Engineering, Iran.

Borja RI, Tamagnini C, Amorosi A (1997) Coupling plasticity and energy-conserving elasticity models for clays. Journal of geotechnical and geoenvironmental engineering 123(10): 948-957

Cil MB, Alshibli KA (2014) 3D evolution of sand fracture under 1D compression. Géotechnique 64(5): 351-364

Collins IF, Houlsby GT (1997) Application of thermomechanical principles to the modelling of geotechnical materials. Proceedings of the Royal Society of London. Series A: Mathematical, Physical and Engineering Sciences 453(1964): 1975-2001

Dafalias YF, Manzari MT (2004) Simple plasticity sand model accounting for fabric change effects. Journal of Engineering mechanics 130(6): 622-634

Einav I (2007a) Breakage mechanics—part I: theory. Journal of the Mechanics and Physics of Solids 55(6): 1274-1297

Einav I (2007b) Breakage mechanics—Part II: Modelling granular materials. Journal of the Mechanics and Physics of Solids 55(6): 1298-1320

Hardin BO, Richart FE (1963) Elastic wave velocities in granular soils. ASCE Journal of the Soil Mechanics and Foundation Division 89(1): 33-65

Hosseininia ES, Mirghasemi AA. (2007) Effect of particle breakage on the behavior of simulated angular particle assemblies. China Particuology 5(5):328-36

Hueckel T (1976) Coupling of elastic and plastic deformations of bulk solids. Meccanica 11(4): 227-235

Hueckel T, Maier G (1977) Incremental boundary value problems in the presence of coupling of elastic and plastic deformations: a rock mechanics oriented theory. International Journal of Solids and Structures 13(1): 1-15

Houlsby GT, Amorosi A, Rojas E. (2005) Elastic moduli of soils dependent on pressure: a hyperelastic formulation. Géotechnique 55(5):383-92.

Hyodo M, Wu Y, Aramaki N, Nakata Y (2017) Undrained monotonic and cyclic shear response and particle crushing of silica sand at low and high pressures. Canadian Geotechnical Journal 54(2): 207-218

Gajo A, Bigoni D, Wood DM (2001) Stress induced elastic anisotropy and strain localisation in sand. In Bifurcation and localisation theory in geomechanics pp 37-44

Golchin A, Lashkari A (2014) A critical state sand model with elastic–plastic coupling. International Journal of Solids and Structures 51(15-16): 2807-2825

Gudehus, G (1979) A comparison of some constitutive laws for soils under radially symmetric loading and unloading. In Proc. Conf. on Num. Meth. in Geomech: 1309-1324

Gudehus, G and Mašín, D (2009) Graphical representation of constitutive equations. Géotechnique, 59(2): 147-151

Guo WL, Zhu JG (2017) Particle breakage energy and stress dilatancy in drained shear of rockfills. Géotechnique Letters 7(4): 304-308

Irani N, Lashkari A, Tafili M, Wichtmann T. (2022) A state-dependent hyperelastic-plastic constitutive model considering shear-induced particle breakage in granular soils. Acta Geotechnica 17(11):5275-98

Irani N, Prada-Sarmiento L.F, Tafili M, Wichtmann T, Triantafyllidis T (2023a) Suitable free energy functions for sand and their application to a bounding surface plasticity model, Suitable free energy functions for sand and their application to a bounding surface plasticity model, submittd version.

Irani N, Tafili M, Sarmiento L.F.P, Wichtmann T (2023b) Breakage indices for crushable materials. Technical Note submitted to Acta Geotechnica.

Karatza Z, Andò E, Papanicolopulos SA, Viggiani G, Ooi JY (2019) Effect of particle morphology and contacts on particle breakage in a granular assembly studied using X-ray tomography. Granular Matter 21(3): 1-13

Mun W, McCartney JS (2017) Roles of particle breakage and drainage in the isotropic compression of sand to high pressures. Journal of Geotechnical and Geoenvironmental Engineering 143(10): 04017071

Niemunis, A. (2008). Incremental Driver User's manual. Available from https://www.soilmodels.com/idriver.

Prada-Sarmiento LF (2011) Paraelastic description of small-strain soil behavior, PhD thesis. Karlsruhe Institute of Technology. https://publikationen.bibliothek.kit.edu/1000028608

Tafili M, Knittel L, Gauger V. (2022). Experimentelle und numerische Untersuchungen zum Kompressionsverhalten von Sand-Schluff-Gemischen. Geotechnik, 45(1): 3-15.

Wichtmann T, Fuentes W, Triantafyllidis T. (2019) Inspection of three sophisticated constitutive models based on monotonic and cyclic tests on fine sand: Hypoplasticity vs. Sanisand vs. ISA. Soil Dynamics and Earthquake Engineering 124:172-83

Xiao Y, Liu H, Chen Y, Chu J (2014) Strength and dilatancy of silty sand. Journal of Geotechnical and Geoenvironmental Engineering 140(7): 06014007

Xiao Y, Liu H, Ding X, Chen Y, Jiang J, Zhang W (2016) Influence of particle breakage on critical state line of rockfill material. International Journal of Geomechanics 16(1): 04015031

Yamamuro JA, Lade PV (1996) Drained sand behavior in axisymmetric tests at high pressures. Journal of Geotechnical Engineering 122(2): 109-119

Yu F (2017) Stress-dilatancy behavior of sand incorporating particle breakage. Acta Geotechnica Slovenica 14(1): 55-61

Yu F (2019) Influence of particle breakage on behavior of coral sands in triaxial tests. International Journal of Geomechanics 19(12): 04019131

Zhang T, Zhang C, Zou J, Wang B, Song F, Yang W. (2020) DEM exploration of the effect of particle shape on particle breakage in granular assemblies. Computers and Geotechnics 122:103542